Int. J. Multiphase Flow Vol. 19, No. 2, pp. 229–243, 1993
Printed in Great Britain.

0301-9322/93 $6.00 + 0.00

RIPPLES GENERATED ON A LIQUID FILM AT HIGH GAS VELOCITIES

J. C. ASALI and T. J. HANRATTY
Department of Chemical Engineering, University of Illinois, Urbana, IL 61801, U.S.A.

(Received 16 April 1991; in revised form 5 September 1992)

Abstract—The growth of capillary ripples on a thin liquid film flowing concurrently with a high velocity gas flow is explored. In particular, a mechanism is examined whereby the ripples receive their energy from pressures and shear stresses exerted at the wave surface by the gas. The predicted wavelength of the most rapidly growing wave is found to be affected by system variables in the same manner as the measured distance between ripple crests. However, the magnitude of the predicted wavelength is one-half the observed wavelength. This could be explained by arguing that finite-amplitude two-dimensional waves are unstable to three-dimensional disturbances which cause alternate peaks and valleys along the crest of the original two-dimensional wave pattern.

Key Words: annular flow, ripple waves, gas–liquid flows, wavelength

1. INTRODUCTION

The wave structure at the interface of a high velocity (>20 m/s) turbulent gas flow and a liquid film flowing along a solid boundary has received considerable attention because of its importance in understanding interfacial stresses in annular flows (Hewitt & Hall-Taylor 1970; Asali *et al.* 1985; Hanratty 1991).

At low liquid flow rates, the film is covered by long-crested slow moving "ripples" having a steep front and a low ratio of the amplitude (10–20 μm) to the wavelength (2–3 mm). Between the ripples the surface is smooth and the flow appears laminar. At sufficiently high liquid flow rates "disturbance" or "roll waves" appear on the film. These have a much larger velocity than the ripples and a very large spacing between successive waves. For flow in a small-diameter pipe the roll waves appear as frothy rings which cover the whole pipe circumference, and the distance between successive waves is several pipe diameters.

In this paper an analysis of the ripple waves is presented. The goals are to identify the physical processes responsible for their appearance and to predict the characteristic distance between them. This length scale is of considerable importance in characterizing interfacial stress in vertical gas–liquid annular flows. For example, Andritsos & Hanratty (1987) and Bontozoglou & Hanratty (1989) have argued that in separated flows the ratio of the interfacial drag to that for a smooth surface should scale with $\Delta h/\lambda$, where Δh is the wave height and λ is the wavelength. Relations for Δh and λ are needed to test this idea.

The approach taken is to solve the linear momentum equations to determine the growth rate of small-amplitude two-dimensional wavelike disturbances at the interface. It is argued that the fastest growing wave is the precursor of the ripples (see Taylor 1963). In carrying out the analysis it is convenient to consider separately the gas and liquid flows. In this framework the gas flow is found to affect the stability of the liquid film through the imposition of pressure and shear forces at the interface. The prediction of the pressure and shear stress variation along a wavy surface over which a turbulent gas is flowing then becomes the central problem in analyzing the growth of small-amplitude disturbances.

The thicknesses of the films on which these ripple waves occur are quite small. For example, at a liquid Reynolds number of 36 and a gas Reynolds number of 78,000, a water film on the wall of a 4.2 cm pipe would have a height of 147 μm. This dictates that the analysis consider wavelengths which are large enough for a shallow-liquid assumption to be made, yet small enough that surface tension effects are important.

It is found that the initial growth of such waves is governed by an imbalance between the destabilizing effects of inertia, the component of the surface shear stress in phase with the wave

slope, the component of the surface pressure in phase with the wave height, and the stabilizing effect of surface tension. These waves, then, seem to fit in the "slow wave" category first discussed by Craik (1966). However, because Craik was concentrating on horizontal flows at much lower gas velocities, the waves being considered in this paper have important differences.

For the conditions at which Craik observed the initiation of "slow waves," stability theory indicates stabilization by both gravity and surface tension and a negligible destabilizing effect of inertia. By carrying out calculations for neutral stability, critical conditions for the appearance of waves are obtained. Instability occurs for arbitrarily thin liquid layers and a critical film height exists, above which the system is stable (as was found by Craik). When calculations are carried out at low gas velocities the results on the critical film height do not agree with the laboratory observations of slow waves by Craik. It, therefore, appears that the stability theory developed by Craik is more applicable to the capillary ripples discussed in this paper than to the "slow waves" discovered by him.

A number of previous authors have described the properties of ripple waves (Würz 1977; Taylor 1963; Shearer & Nedderman 1965). However, the only systematic results on the influence of flow variables on the wavelength have been given by Würz (1977) in his study of a water film flowing along the bottom wall of a horizontal rectangular 25 × 60 mm channel through which air at velocities of 68.1, 118.9 and 173.8 m/s was flowing. The results of the analysis are compared with these measurements of Würz (1977) as well as with measurements by Asali (1984) for the concurrent flow of liquid films, with viscosities of 1.1 and 2.0 cP, and air, with velocities of 28.9, 40.9, 48.2 and 56.1 m/s up a 4.2 cm tube.

A principal finding in this paper is that the ripple waves are primarily associated with wave-induced gas-phase shear stress variations. We conclude that nonlinear processes cause two-dimensional unstable waves to develop into a three-dimensional wave pattern with a distance between crests equal to twice the wavelength of the initial instability, since ripple spacings calculated in this way are very close to measurements. It is found that the ratio of the ripple spacing to the height of the wall film is a function of three dimensionless groups: the liquid film Reynolds number, $(\mu_L \rho_G^{1/2}/\mu_G \rho_L^{1/2})$ and $(\sigma/v_G^* \mu_G)$. The results are probably too complicated to use directly, so their main value will be in guiding the development of empirical relations.

Details on the analysis and on the experiments may be found in a thesis by one of the authors (Asali 1984). The method of analysis is also outlined in a review article (Hanratty 1983) in which a mechanism is proposed for the generation of capillary ripples on thin films. This paper gives a much more detailed account of the evidence supporting this proposition. Attention is called to recent papers by Jurman & McCready (1989) and by Jurman *et al.* (1989) which expand on the analyses of thin films presented by Hanratty (1983).

2. ANALYSIS

(a) Equation for the complex wave velocity

A disturbance of the form

$$h' = a \exp i\alpha(x - Ct) \qquad [1]$$

is imposed on the interface of the fully developed gas–liquid flow depicted in figure 1. Here h' is the displacement of the interface from its time-averaged location, x is the distance in the direction

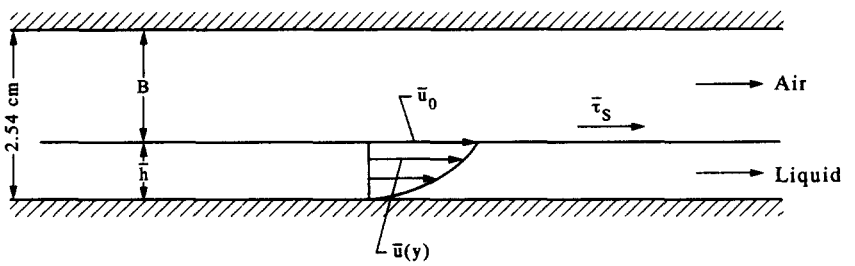

Figure 1. System being analyzed.

of flow and t is the time. The amplitude of the disturbance, a, and the wavenumber, $\alpha = 2\pi/\lambda$, are real positive quantities. The wave velocity, C, is complex,

$$C = C_R + iC_I, \tag{2}$$

and the most rapidly growing wave is the one for which αC_I is a maximum.

The velocity in the liquid film, $u(y)$, varies from zero at the wall, $y = 0$, to a maximum at the interface, $y = h$. An average velocity and a shape factor are defined as

$$u_a = \frac{1}{h}\int_0^h u \, dy \tag{3}$$

and

$$\Gamma = \frac{1}{hu_a^2}\int_0^h u^2 \, dy. \tag{4}$$

The interfacial wave is accompanied by two-dimensional disturbances in the fully developed velocity fields, in the gas-phase pressure and shear stress at the interface and in the shear stress at the wall.

The amplitude of the wave is assumed small enough that it induces a linear response in the velocity and stress fields, so that the disturbances can be represented as

$$\frac{u'_a}{\hat{u}_a} = \frac{\Gamma'}{\hat{\Gamma}} = \frac{P'_S}{\hat{P}_S} = \frac{\tau'_S}{\hat{\tau}_S} = \frac{\tau'_W}{\hat{\tau}_W} = a \exp i\alpha(x - Ct). \tag{5}$$

The amplitudes $a\hat{u}_a$, $a\hat{\Gamma}$, $a\hat{\tau}_S$, $a\hat{P}_S$ and $a\hat{\tau}_W$ are complex. Thus, if only the real parts of [1] and [5] are considered,

$$h' = a \exp(\alpha C_I t)\cos\alpha(x - C_R t), \tag{6}$$

$$P'_S = a \exp(\alpha C_I t)[\hat{P}_{SR}\cos\alpha(x - C_R t) - \hat{P}_{SI}\sin\alpha(x - C_R t)] \tag{7}$$

and

$$\tau'_S = a \exp(\alpha C_I t)[\hat{\tau}_{SR}\cos\alpha(x - C_R t) - \hat{\tau}_{SI}\sin\alpha(x - C_R t)]. \tag{8}$$

The amplitudes $a\hat{P}_{SR}$ and $a\hat{\tau}_{SR}$ are the components of P'_S and τ'_S in phase with the wave amplitude; the amplitudes $a\hat{P}_{SI}$ and $a\hat{\tau}_{SI}$ are the components in phase with the wave slope.

An equation for C, in terms of $\hat{u}_a$, $\hat{\Gamma}$, $\hat{P}_S$, $\hat{\tau}_S$ and $\hat{\tau}_W$ is obtained from a consideration of integral forms of the mass and momentum balance equations for the film. These balance equations are simplified by making a shallow-water assumption, whereby the pressure in the liquid is given as

$$P = P_S + g(h - y)\rho_L \sin\beta - \sigma\frac{\partial^2 h}{\partial x^2}, \tag{9}$$

where σ is the surface tension, g is the acceleration of gravity, ρ_L is the liquid density and β is the inclination of the channel.

The accuracy of [9] depends on an assumption similar to that made in boundary-layer theory since wavelength, λ, and film height, $\bar{h}$, characterize spatial variations in the x- and y-directions. By applying such scaling to the Navier–Stokes equations, it is found (as in boundary-layer theory) that the ratio of the inertia terms in the y-momentum equation to the inertia terms in the x-momentum equation is of the order $(\alpha\bar{h})$. Furthermore, the ratio of the viscous terms to the inertia terms in the y-momentum equation is of the order $(\alpha\bar{h}\mathrm{Re}_L)^{-1}$, where Re_L is the film Reynolds number defined as $(\bar{h}\bar{u}_a)/\nu_L$. Equation [9] is then obtained by integrating the y-momentum equation, assuming $\alpha\bar{h}\mathrm{Re}_L$ is of order unity or greater and that terms of order $(\alpha\bar{h})^2$ can be neglected. A formal derivation of this result can be found in the paper by Alekseenko *et al.* (1985), which also presents a justification for using integral methods to calculate waves on thin liquid films.

The following equation for the complex wave velocity is obtained by Hanratty (1983) after linearizing these integral balance equations and substituting [5]:

$$C^2 + \bar{u}_a^2\bar{\Gamma} - 2\bar{u}_a\bar{\Gamma}C - \bar{h}\bar{u}_a^2\hat{\Gamma} = i\frac{\hat{\tau}_S}{\rho_L\alpha} - i\frac{\hat{\tau}_W}{\rho_L\alpha} - \frac{i(\bar{\tau}_S - \bar{\tau}_W)}{\alpha\bar{h}\rho_L} + \bar{h}\frac{\hat{P}_S}{\rho_L} + g\bar{h}\sin\beta + \frac{\alpha^2\sigma\bar{h}}{\rho_L}. \tag{10}$$

The quantities on the left-hand side of [10] represent the inertia terms. For a plug flow in the film ($\bar{\Gamma} = 1$ and $\hat{\Gamma} = 0$) they are equal to $(\bar{u}_a - C)^2$ and, consequently, always destabilizing. For $\bar{u}_a = C$ the effects of inertia vanish for a plug flow. They also vanish for $C = 2\bar{u}_a$ and $\bar{\Gamma} = 4/3$. However, in general, inertia can be stabilizing or destabilizing.

The real and imaginary parts of [10] yield two equations defining C_R and C_I:

$$-C_I^2 + C_R^2 - 2\bar{\Gamma}\bar{u}_a C_R + \bar{\Gamma}\bar{u}_a^2 - \bar{h}\bar{u}_a^2\hat{\Gamma}_R = -\frac{\hat{\tau}_{SI}}{\rho_L\alpha} + \frac{\hat{\tau}_{WI}}{\rho_L\alpha} + \frac{\alpha\bar{h}\hat{P}_{SR}}{\rho_L\alpha} + g\bar{h}\sin\beta + \frac{\alpha^2\sigma\bar{h}}{\rho_L} \quad [11]$$

and

$$-\bar{h}\bar{u}_a^2\hat{\Gamma}_I + 2C_I(C_R - \bar{\Gamma}\bar{u}_a) = \frac{\hat{\tau}_{SR}}{\alpha\rho_L} - \frac{\hat{\tau}_{WR}}{\alpha\rho_L} - \frac{(\bar{\tau}_S - \bar{\tau}_W)}{\alpha\bar{h}\rho_L} + \frac{\alpha\bar{h}\hat{P}_{SI}}{\rho_L\alpha}, \quad [12]$$

with

$$\frac{\bar{\tau}_S - \bar{\tau}_W}{\bar{h}} = \frac{d\bar{P}}{dx} - \rho_L g\cos\beta = \bar{\bar{p}}. \quad [13]$$

Since $\hat{\tau}_{WR}$ is strongly related to C_R, [12] may be viewed as defining C_R under neutral stability conditions ($C_I = 0$). This velocity is the kinematic wave velocity defined by Lighthill & Whitman (1955). In this context, [11] then defines the dynamic conditions necessary for neutral stability.

It is to be noted in [11] and [12] that as $\alpha\bar{h}$ becomes smaller, for a fixed gas velocity, $\hat{\tau}_{SR}$ and $\hat{\tau}_{SI}$ become more important relative to $\hat{P}_{SR}$ and $\hat{P}_{SI}$. The reason for this, as pointed out by Cohen & Hanratty (1965), is that $\hat{P}$ and $\hat{\tau}$, respectively, feed energy into the film through normal velocity fluctuations and tangential velocity fluctuations. As $\alpha\bar{h}\to 0$ the ratio of the normal to the tangential velocity fluctuations in the film also approaches zero.

In order to use [11] and [12] to calculate the fastest growing wave it is necessary to develop relations for $\hat{\tau}_S$, $\hat{P}_S$, $\hat{\tau}_W$ and $\hat{\Gamma}$.

(b) Evaluation of $\hat{P}_S$ and $\hat{\tau}_S$

The complex amplitudes $a\hat{\tau}_S$ and $a\hat{P}_S$ are determined from a solution of the linearized momentum equations for the gas. The gas streamlines are compressed in the crest region and are expanded in the trough region. Thus, according to the Bernoulli equation, one expects $\hat{P}_{SR}$ to be negative and destabilizing; i.e. it will supply a suction at the crest. Similarly, because of the compression of the streamlines at the crest, $\hat{\tau}_{SR}$ will be positive. Calculations by Benjamin (1959) indicate that the maximum in the shear stress occurs upstream of the crest, $\hat{\tau}_{SI}$ = plus value, and that the minimum pressure occurs downstream of the crest, $\hat{P}_{SI}$ = plus value. As depicted in figure 2, a positive $\hat{\tau}_{SI}$ would be destabilizing. For a wave propagating in the positive x-direction, a positive $\hat{P}_{SI}$ is destabilizing in that it is accompanied by a transmission of energy from the gas phase to the disturbance in the liquid.

Most of the theoretical analyses of interfacial instabilities have used the solution by Benjamin (1959), which neglects the effect of turbulence on the wave-induced flow, to predict $\hat{P}_S$ and $\hat{\tau}_S$. Benjamin formulated the linear momentum equations for the gas flow in a curvilinear coordinate system which conforms to a small-amplitude sinusoidal wave at the gas–liquid interface. However,

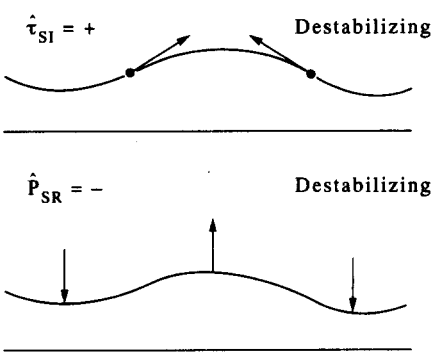

Figure 2. Influence of surface stresses on stability.

the nonhomogeneous terms in the momentum equations introduced because of the use of curvilinear coordinates were neglected, so that the expressions derived for $\hat{\tau}_S$ and $\hat{P}_S$ are the same as would be obtained if the problem were formulated in a cartesian coordinate system. Thorsness *et al.* (1978) have examined possible errors caused by the neglect of turbulence effects and by the use of a Cartesian coordinate system. It was found that these assumptions are valid only for large values of the dimensionless wavenumber $\alpha_G^+ = \nu_G \alpha / v_G^*$, where ν_G is the kinematic viscosity of the gas and $v_G^* = (\bar{\tau}_S/\rho_G)^{1/2}$ is the gas-phase friction velocity. In the range of α_G^+ of interest in the present analysis, considerable errors can be made in evaluating $\hat{\tau}_{SR}$ and $\hat{\tau}_{SI}$ using the results presented by Benjamin (1959).

The calculations in this paper use a slight modification of the Model D explored by Thorsness *et al.* (1978). This approach is the relaxation analysis of Abrams & Hanratty (1984) or Model D* in Abrams (1984). It uses a boundary-layer coordinate system embedded in the wave surface and a modification of the van Driest mixing length model outlined by Loyd *et al.* (1970).

Values of the amplitude and the phase angle characterizing the calculated variation of τ_S and P_S, given as the solid lines in figures 3 and 4, agree with measurements of τ_S along a solid wavy surface for $\alpha_G^* = 4 \times 10^{-4}$ to 10^{-2}. The amplitude is defined as

$$|\hat{\tau}_S| = (\hat{\tau}_{SR}^2 + \hat{\tau}_{SI}^2)^{1/2}, \qquad [14]$$

with

$$\hat{\tau}_{SR} = |\hat{\tau}_S| \cos \Theta_\tau \qquad [15]$$

and

$$\hat{\tau}_{SI} = |\hat{\tau}_S| \sin \theta_\tau. \qquad [16]$$

The dashed curves in figures 3 and 4 were calculated using a cartesian coordinate system and a quasi laminar assumption (the Benjamin solution in a cartesian coordinate system). Since the wave velocities are so small these results for solid waves are used to evaluate $\hat{\tau}_S$ and $\hat{P}_S$ appearing in [10]. It is encouraging that Jurman *et al.* (1989) obtained good agreement with experiments when they used Abram's analysis for the gas phase in their studies of waves on liquid films.

(c) Evaluation of $\hat{\tau}_w$ and $\hat{\Gamma}$

For disturbances of very long wavelengths ($\alpha \bar{h}$ small) the change of height of the liquid with distance is gradual enough that the shape of the velocity profile can be closely approximated by that which would exist for a flow without a disturbance. Therefore, $\hat{\tau}_W$ and $\hat{\Gamma}$ are evaluated by assuming the relationships of τ_W and Γ with u_a and h are the same as would be determined for an undisturbed flow. Furthermore, the film, on which the ripple waves appear, may be considered laminar. Details regarding these calculations are presented by Hanratty (1983).

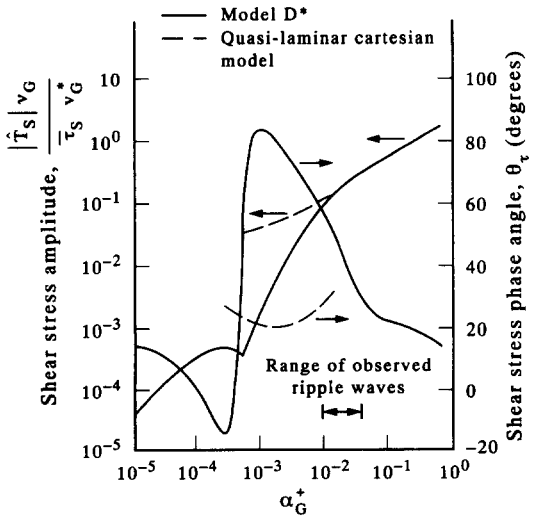

Figure 3. Wave-induced variation of the surface shear stress.

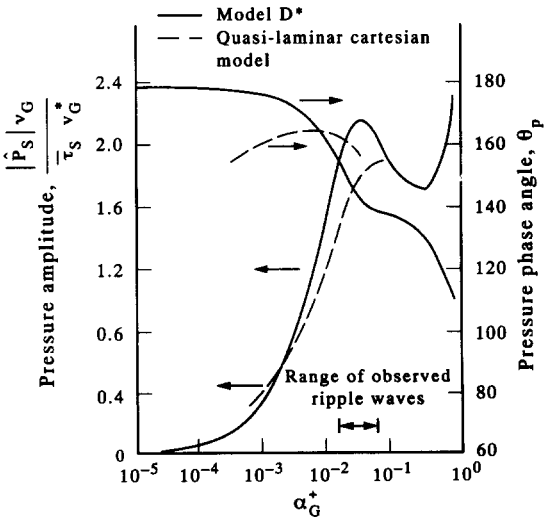

Figure 4. Wave-induced variation of the surface pressure.

(d) Relations for wave growth

For gas flows over very thin films at high gas velocities a number of simplifications in the analysis can be made. Since the flow is laminar the average velocity at the interface, $\bar{u}_S$, is equal to $2\bar{u}_a$, $\bar{\tau}_S \cong \bar{\tau}_W = 2\bar{u}_a\mu_L/\bar{h}$. This means that $\bar{\tau}_S/\rho\bar{u}_a^2 = 2/\mathrm{Re}_L$. Furthermore, from [13] it is seen that for fully developed horizontal flow the group $\mathbf{P} = \bar{P}\bar{h}^2/\mu_L u_a$ may be approximated as $2(\bar{\tau}_S - \bar{\tau}_W)/\bar{\tau}_W$ so that $\mathbf{P} \cong -2\bar{h}/H$, where H is the half height of the gas space. The same estimate can be applied to vertical pipes where $\bar{P} \cong \mathrm{d}\bar{P}/\mathrm{d}x$. For the high velocity gas flows considered in this paper $2\bar{h}/H$ is of the order 1.5×10^{-3}. As a consequence, the term $(\bar{\tau}_S - \bar{\tau}_W)/\alpha\bar{h}\rho_L$ in [12] and terms containing $\mathbf{P}$ in the estimates of $\bar{\Gamma}$, $\hat{\tau}_W$ and $\hat{\Gamma}$ can be neglected.

The following approximations can, therefore, be made for small $\alpha\bar{h}$ (see Hanratty 1983):

$$\frac{\bar{h}\hat{\tau}_W}{\bar{\tau}_S} = \frac{3}{2}\left(\frac{C}{\bar{u}_a} - 2\right) - \frac{1}{2}\frac{\bar{h}\hat{\tau}_S}{\bar{\tau}_S}. \qquad [17]$$

For small $\alpha\bar{h}$ and small $\bar{h}/H$,

$$\bar{h}\hat{\Gamma} = \frac{1}{270}\left(90 - \frac{45C}{\bar{u}_a}\right) + 3\frac{\hat{\tau}_S\bar{h}}{\bar{\tau}_S}, \quad \bar{\Gamma} = \frac{4}{3}. \qquad [18]$$

If [17] and [18] are substituted into [11] and [12], the following relations for C_R and C_I are obtained:

$$\frac{C_R}{\bar{u}_a}\left[1 + \frac{2}{3}\mathrm{Re}_L(\alpha\bar{h})\frac{C_I}{\bar{u}_a}\right] = 2\left[1 + \frac{5}{12}\mathrm{Re}_L(\alpha\bar{h})\frac{C_I}{\bar{u}_a}\right] + (\alpha\bar{h})\left[\frac{\hat{\tau}_{SR}}{\alpha\bar{\tau}_S} + \frac{2}{3}(\alpha\bar{h})\frac{\hat{P}_{SI}}{\alpha\bar{\tau}_S} - \frac{1}{18}(\alpha\bar{h})\mathrm{Re}_L\frac{\hat{\tau}_{SI}}{\alpha\bar{\tau}_S}\right] \qquad [19]$$

and

$$-\left(\frac{C_I}{\bar{u}_a}\right)^2 + \left(\frac{C_R}{\bar{u}_a}\right)^2 - \frac{5}{2}\left(\frac{C_R}{\bar{u}_a}\right) + 1 - \frac{1}{6}(\alpha\bar{h})\frac{\hat{\tau}_{SR}}{\alpha\bar{\tau}_S}$$

$$= -\frac{2}{\mathrm{Re}_L}\left[\frac{3}{2}\frac{\hat{\tau}_{SI}}{\alpha\bar{\tau}_S} - (\alpha\bar{h})\frac{\hat{P}_{SR}}{\alpha\bar{\tau}_S} - \frac{\rho_L g\bar{h}}{\bar{\tau}_S}\sin\beta - \frac{(\alpha\bar{h})^2\sigma}{\bar{\tau}_S\bar{h}}\right] + \frac{3}{\mathrm{Re}_L(\alpha\bar{h})}\frac{C_I}{\bar{u}_a}, \qquad [20]$$

where $\mathrm{Re}_L = hu_a/\nu_L$ is the liquid film Reynolds number. (Equations [19] and [20] are obtained from [5.3] and [5.4] in Hanratty (1983) if $\mathbf{P} = 0$ and $\bar{\tau}_S = \rho\bar{u}_a^2$ are substituted.)

Equations [19] and [20] can be further simplified if terms multiplied by $(\alpha\bar{h})$ and $(\alpha\bar{h})\mathrm{Re}_L$ can be ignored. The following results are obtained:

$$\frac{C_R}{\bar{u}_a} = 2 \qquad [21]$$

and

$$0 = \frac{-2}{\mathrm{Re}_L}\left[\frac{3}{2}\frac{\hat{\tau}_{SI}}{\alpha\bar{\tau}_S} - (\alpha\bar{h})\frac{\hat{P}_{SR}}{\alpha\bar{\tau}_S} - \frac{\rho_L g\bar{h}}{\bar{\tau}_S}\sin\beta - \frac{(\alpha\bar{h})^2\sigma}{\bar{\tau}_S\bar{h}}\right] + \frac{3}{\mathrm{Re}_L\alpha\bar{h}}\frac{C_I}{\bar{u}_a}. \qquad [22]$$

It is to be noted in this case that the inertia terms vanish. They are neither stabilizing nor destabilizing.

This simplification can lead to error for high velocity gas flows, the case being considered in this paper. Under these circumstances, one can have a large Re_L even though the film is very thin. From figures 3 and 4 the following estimates can be made in the range of α_G^+ of interest to this problem:

$$\frac{\hat{\tau}_{SR}}{\alpha\bar{\tau}_S} \cong \frac{\hat{\tau}_{SI}}{\alpha\bar{\tau}_S} \cong 7, \quad \frac{\hat{P}_{SR}}{\alpha\bar{\tau}_S} \cong -78, \quad \frac{\hat{P}_{SI}}{\alpha\bar{\tau}_S} \cong +45. \qquad [23]$$

The film thickness is of the order of 10^{-3} cm, the wavelength 10^{-1} cm and $(\alpha\bar{h}) \cong 0.06$. Therefore, terms involving $\hat{\tau}_{SI}$ and $\hat{P}_{SR}$ could be of equal importance in [20] and $\hat{\tau}_{SR}$ is slightly more important than $\hat{P}_{SI}$ in [19]. From [23] it is estimated that

$$\alpha\bar{h}\frac{\hat{\tau}_{SR}}{\alpha\bar{\tau}_S} \cong 0.4 \qquad [24]$$

This indicates that, unless $\alpha\bar{h}\mathrm{Re}_L$ is a large number, $C_R/\bar{u}_a$ is slightly larger than 2. Because of this, the inertia terms

$$\left[\left(\frac{C_R}{\bar{u}_a}\right)^2 - \frac{5}{2}\left(\frac{C_R}{\bar{u}_a}\right) + 1\right]$$

in [20], under most circumstances, are greater than zero. This can be an important destabilizing effect.

For a vertical flow the gravity term in [20] is identically zero so that surface tension is the only stabilizing influence. For the range of conditions covered in the experiments of Würz (1977) in a horizontal channel, it is also found that the surface tension term is far more important than gravity.

Therefore, the picture that emerges from a consideration of [19] and [20] is as follows. Wave growth (C_I = plus value) is governed by the imbalance between the destabilizing effects of inertia, $\hat{\tau}_{SI}$ and $\hat{P}_{SR}$, and the stabilizing effect of surface tension. Inertia is usually destabilizing because $\hat{\tau}_{SR}$ and $\hat{P}_{SI}$ cause the wave velocity, as defined by [19], to be greater than the velocity of the liquid at the interface. The terms involving $\hat{\tau}_{SR}$, $\hat{\tau}_{SI}$, $\hat{P}_{GR}$ and $\hat{P}_{GI}$ are functions of $\alpha_G^+ = (\alpha\bar{h})/(h_G^+)$. For thin laminar films, $h_G^+ = 1.414\mathrm{Re}_L^{0.5}(\mu_L\rho_G^{1/2}/\mu_G\rho_L^{1/2})$. Therefore, [19] and [20] indicate that

$$\frac{C_R}{\bar{u}_a} = f_1\left(\alpha\bar{h}, \frac{\sigma}{v_G^*\mu_G}, \mathrm{Re}_L, \frac{\mu_L\rho_G^{1/2}}{\mu_G\rho_L^{1/2}}\right) \qquad [25]$$

and

$$\frac{C_I}{\bar{u}_a} = f_2\left(\alpha\bar{h}, \frac{\sigma}{v_G^*\mu_G}, \mathrm{Re}_L, \frac{\mu_L\rho_G^{1/2}}{\mu_G\rho_L^{1/2}}\right). \qquad [26]$$

3. MEASUREMENTS OF WAVELENGTHS

Measurements of wavelengths of capillary ripples observed on thin liquid layers at high gas velocities were made in a facility built by Asali (1984) and described by Asali *et al.* (1985). Air and liquid flowed vertically up a 4.2 cm plexiglass tube that is 9 m long and has dia = 4.2 cm. Water (1.1 cP) or a water–glycerine solution (2.0 cP) were introduced into the pipeline through a slot which admitted the liquid as an annular film along the wall at a small enough rate that no liquid was entrained in the gas. The pipe emptied into a 15.2 cm dia cylindrical manifold, 1.72 m long, which was connected to a separator to remove liquid from the air that discharges into the laboratory. The liquid was recirculated through a shell and tube heat exchanger to control the temperature.

The pressure drop was measured by using two liquid-filled manometers. Each had one side connected to a pressure tap in the test section and the other to a pressure tap in the separator. The pressure drop is calculated as the difference between the readings of these two manometers. The gauge pressure was measured by using another manometer with one side connected to the top in the separator and the other open to the atmosphere. A small continuous liquid purge was used to prevent air bubbles from entering the leads to the pressure taps.

Average liquid film thicknesses, $\bar{h}$, were determined by measuring the conductance between two electrodes mounted flush with the pipe wall. Details regarding these measurements are given by Asali *et al.* (1985).

The average stress at the interface, $\bar{\tau}_S$, was calculated, from the measurements of the pressure gradient and the film height, with the equation

$$\bar{\tau}_S = \left(\frac{d_t - 2\bar{h}}{4}\right)\frac{d\bar{P}}{dx}, \qquad [27]$$

where d_t is the tube diameter.

The ripples appearing on the liquid could be seen through the transparent pipe wall. They were photographed on 35 mm film and magnified approx. 17 times using a slide projector. Typical photographs of the waves are shown in figure 5 for a water film and in figure 6 for a liquid film with a viscosity of 2.0 cP. The spacing between ripples in the central portion, where there was little distortion because of the pipe curvature, were measured with a meter stick. An arithmetic mean

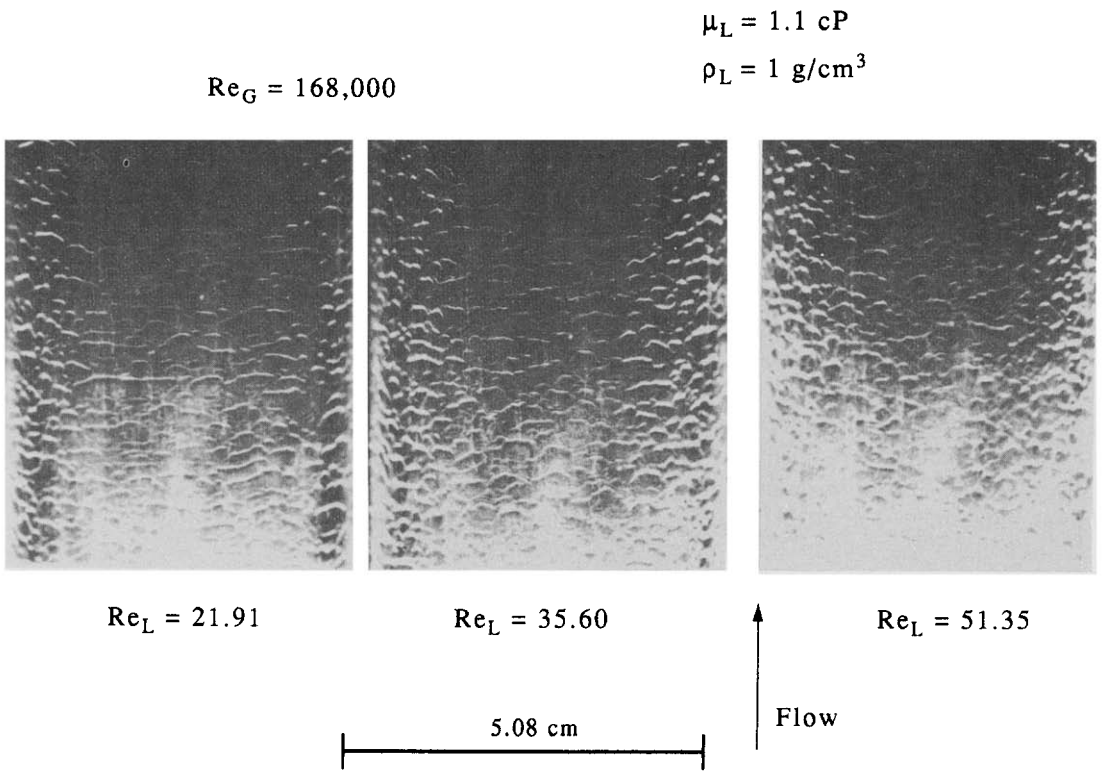

Figure 5. Ripple waves on a water film.

of the separation distance of these ripples for a fixed liquid and gas flow rate was then reported as the wavelength.

Measurements of the wavelengths, obtained in this way are summarized in tables 1 and 2 and in figures 7 and 8, where the curves are best fits of the data.

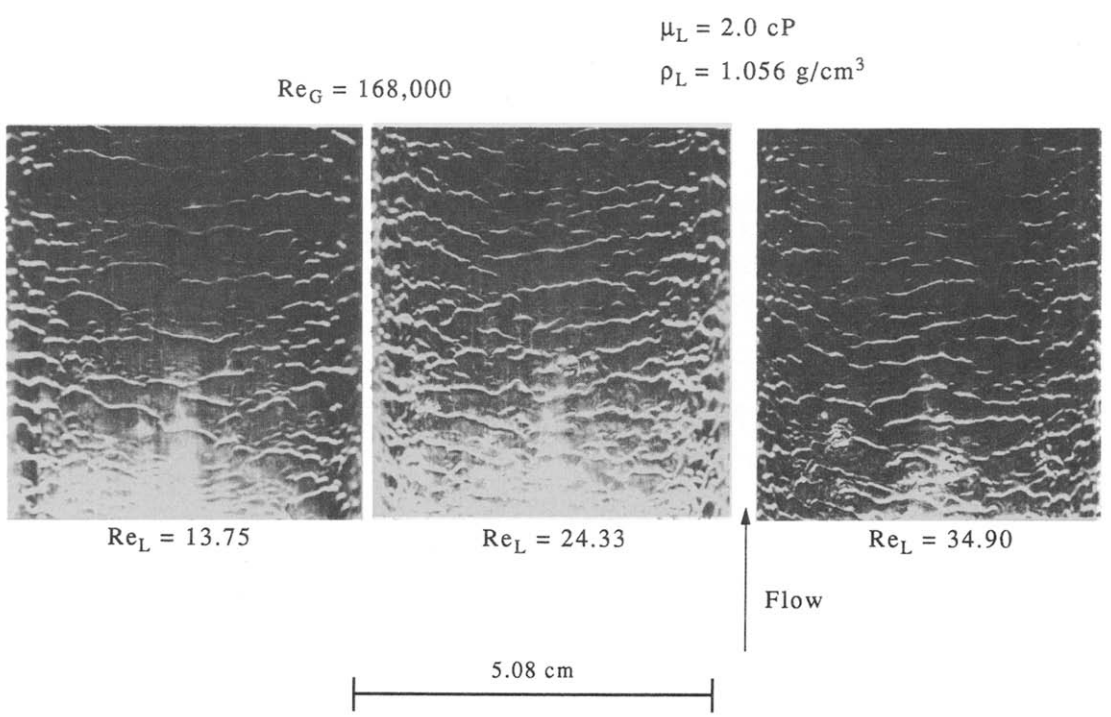

Figure 6. Ripple waves on a liquid film with a viscosity of 2.0 cP.

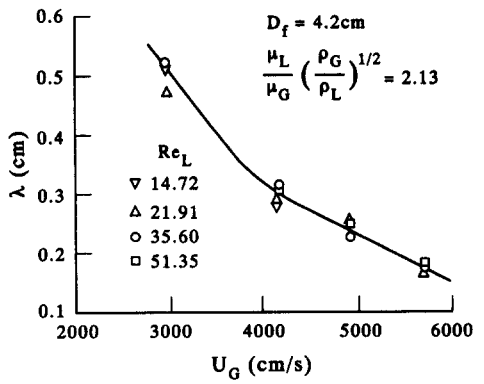

Figure 7. Measured average spacing between ripples for a water film with a viscosity of 1.1 cP.

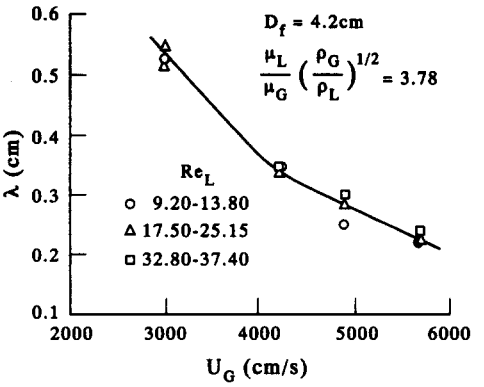

Figure 8. Measured average spacing between ripples for a liquid film with a viscosity of 2.0 cP.

Würz (1977) obtained similar measurements for air–water flow in a horizontal rectangular enclosed channel that was 2.54 cm high. Some of his results are summarized in table 3.

4. RESULTS

(a) Numerical calculations

Typical values of $(\alpha\bar{h})\mathrm{Re}_L(C_1/\bar{u}_a)$ calculated from [19] and [20] are shown in figure 9 for a fixed value of $(\mu_L\rho_G^{1/2})/(\mu_G\rho_L^{1/2})$ and $\sigma/(v_G^*\mu_G)$. From such a plot, values of $(\alpha\bar{h})$ corresponding to the maximum wave growth can be calculated.

Figures 10 and 11 present values of $(\alpha\bar{h})_{max}$ for fixed values of $(\mu_L\rho_G^{1/2})/(\mu_G\rho_L^{1/2})$ corresponding to the water and the water–glycerine solutions that were studied (see tables 1 and 2). Figures 12

Table 1. Ripple wave data obtained for air–water flows in a 4.2 cm vertical pipe ($\rho_L = 0.99$ g/cm^3 and $\mu_L = 1.1$ cP)

Re_G	Re_L	$\bar{h}$ (cm)	ρ_G (g/cm^3)	λ observed (cm)	2λ predicted (cm)
168,000	21.91	5.0×10^{-3}	1.32×10^{-3}	0.174	0.17
	35.6	6.0×10^{-3}		0.188	0.19
	51.35	7.2×10^{-3}		0.176	0.22
140,000	21.91	6.5×10^{-3}	1.28×10^{-3}	0.257	0.23
	35.6	8.0×10^{-3}		0.233	0.27
	51.35	9.2×10^{-3}		0.252	0.30
115,000	14.72	6.0×10^{-3}	1.24×10^{-3}	0.28	0.25
	21.91	7.9×10^{-3}		0.292	0.30
	35.6	9.7×10^{-3}		0.318	0.35
	51.35	11.6×10^{-3}		0.309	0.40
78,100	14.72	10.5×10^{-3}	1.19×10^{-3}	0.509	0.50
	21.91	11.87×10^{-3}		0.465	0.52
	35.6	14.73×10^{-3}		0.518	0.59

Table 2. Ripple wave data obtained for air–glycerine solution in a 4.2 cm pipe ($\rho_L = 1.056$ g/cm^3 and $\mu_L = 2.0$ cP)

Re_G	Re_L	$\bar{h}$ (cm)	ρ_G (g/cm^3)	λ observed (cm)	$\lambda/\bar{h}$	2λ predicted (cm)	$\alpha\bar{h}$	$(\alpha\bar{h})Re_L$
168,000	13.75	6.3×10^{-3}	1.32×10^{-3}	0.221	35	0.17	0.18	2.5
	24.33	8.3×10^{-3}		0.227	27	0.20		
	34.9	10.0×10^{-3}		0.239	24	0.24	0.26	9.1
139,000	9.17	6.2×10^{-3}	1.27×10^{-3}	0.252	40.1	0.19	0.16	1.4
	23.27	9.4×10^{-3}		0.286	30.4	0.24		
	37.35	12.9×10^{-3}		0.302	23	0.34	0.27	10.2
116,000	9.9	7.6×10^{-3}	1.20×10^{-3}	0.345	45	0.25	0.14	1.4
	24.12	11.0×10^{-3}		0.343	31	0.31		
	32.78	12.8×10^{-3}		0.344	27	0.36	0.23	7.6
78,000	9.9	12.7×10^{-3}	1.19×10^{-3}	0.524	41	0.40	0.15	1.5
	17.53	15.6×10^{-3}		0.516	33	0.54		
	25.15	18.4×10^{-3}		0.547	30	0.56	0.21	5.3

Table 3. Ripple wave data obtained by Würz (1977) for air–water in a 2.54 cm horizontal channel ($\rho_L = 1.0$ g/cm^3 and $\rho_G = 1.25 \times 10^{-3}$ g/cm^3)

Re_L	$\bar{h}$ (cm)	μ_L (cP)	λ observed (cm)	2λ predicted (cm)
8.2	3.9×10^{-3}	1.05	0.145	0.145
17	5.8×10^{-3}		0.165	0.165
27	7.4×10^{-3}		0.177	0.185
56	10.9×10^{-3}		0.175	0.258
9.1	2.8×10^{-3}	1.20	0.085	0.079
19	4.1×10^{-3}		0.096	0.084
30	5.3×10^{-3}		0.091	0.084
40	6.2×10^{-3}		0.09	0.114
45	1.5×10^{-3}	1.27	0.06	0.043
11	2.3×10^{-3}		0.062	0.046
20	3.1×10^{-3}		0.058	0.057
35	4.2×10^{-3}		0.056	0.068

and 13 present calculated values of $(C_R/\bar{u}_a)$ at $(\alpha\bar{h})_{max}$. It noted that except for the largest Re_L, $(C_R/\bar{u}_a)$ is greater than 2 and independent of surface tension. This is consistent with the physical picture that the waves are kinematic, rather than dynamic.

(b) Comparison of theory with measurements

A comparison of the calculated values of λ_{max} and the measured λ is given in figure 14 and in tables 1 and 2. It is noted that the measured λ are twice the calculated λ for the maximum growth of two-dimensional waves.

The calculations shown in figures 9–13 used the assumption of a steady laminar flow to develop the relationship between the film flow rate and the film height given before [25]. It is assumed that this relation still holds locally for films with waves then the time-averaged height is given as

$$\overline{h_G^+} = \frac{\bar{h}}{(\overline{h^2})^{1/2}} 1.415 Re_L^{0.5} \left[\frac{\mu_L \rho_G^{1/2}}{\mu_G \rho_L^{1/2}}\right]. \qquad [28]$$

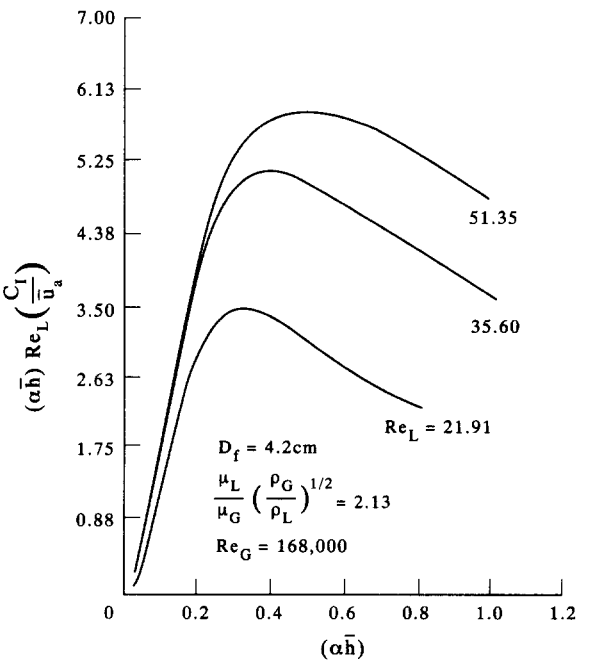

Figure 9. Typical examples of values of calculated growth rates of disturbances.

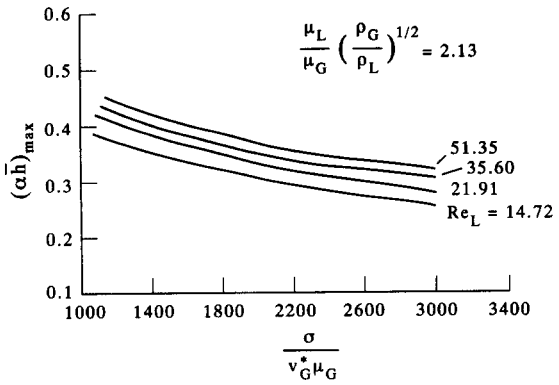

Figure 10. Calculated wavelengths of maximum growth for a water film.

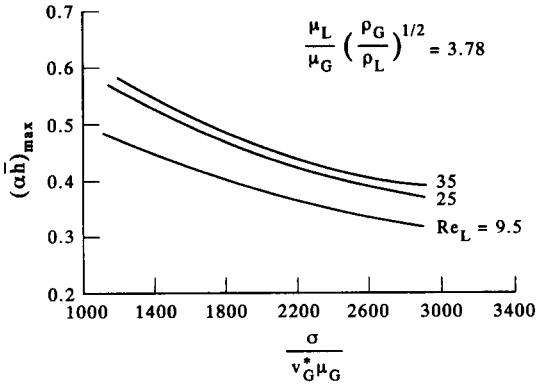

Figure 11. Calculated wavelengths of maximum growth for a 2.0 cP film.

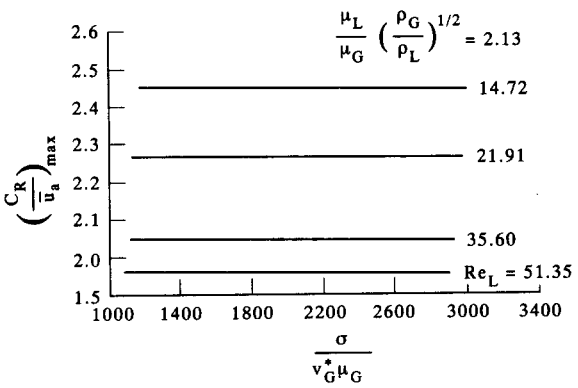

Figure 12. Calculated velocities of the fastest growing waves on a water film.

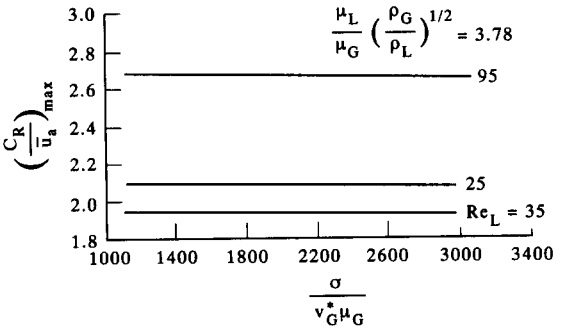

Figure 13. Calculated velocities of the fastest growing waves on a liquid film with a viscosity of 2.0 cP.

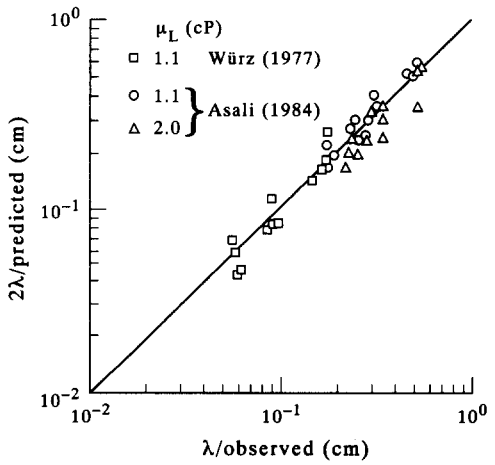

Figure 14. Comparison of calculated and measured spacings of the most rapidly growing waves.

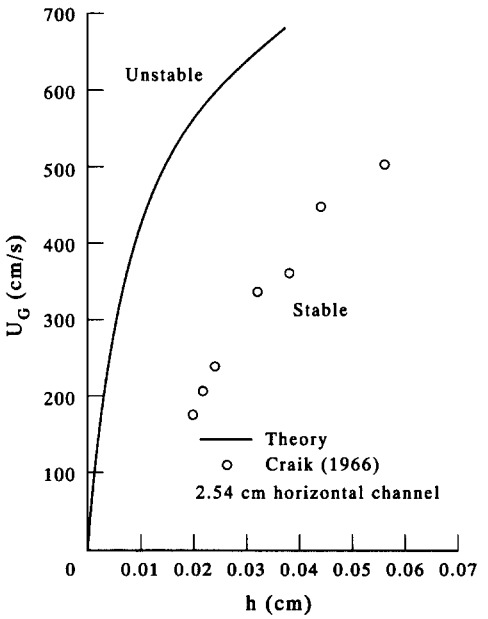

Figure 15. Comparison of the neutral stability line for a horizontal flow at low gas velocities with the transition observed by Craik (1966).

Measurements by Asali *et al.* (1985) for the thin films that exist in annular flow give

$$h_G^+ = 0.781 \mathrm{Re}_L^{0.6}\left(\frac{\mu_L \rho_G^{1/2}}{\mu_G \rho_L^{1/2}}\right). \quad [29]$$

If this value of the film height were used in the calculations the spread of the data points around the relation 2λ predicted $= \lambda$ observed is less than is shown in figure 14.

(c) Comparison of stability theory with "slow" waves observed by Craik (1966)

At low gas velocities, [19] and [20] predict a critical film height in a horizontal channel above which the film is stable, as shown in figure 15. This type of behavior was predicted by Craik (1966). The chief difference in the calculated results presented in figure 15 and the results presented by Craik is that more accurate values of $\hat{\tau}_S$ and $\hat{P}_S$ are used.

Also shown in figure 15 are experimental observations by Craik of the critical film heights below which a long-wavelength disturbance appeared on the film.

Craik (1966) reported results for a 2.54 cm channel, in which the ratio of the wavelength to the height of the channel was approx. 0.7 and for a 15.24 cm channel. Only the results for the 2.54 cm test section are compared to the calculations because the experiments on which the estimates of $\hat{\tau}_S$ are based were done with a wavelength to channel height ratio of 1. The gas velocity plotted in figure 15 is the bulk velocity. The centerline velocity reported in figure 5 of Craik's paper was multiplied by a factor, which varied between 0.71 and 0.78, to obtain U_G.

Craik (1966) used the quasi-laminar model of Benjamin to estimate $\hat{\tau}_S$ and predicted a transition at much smaller liquid heights for the 2.54 cm channel (see figure 11 of his paper) than was observed. The calculations presented in figure 15, using a more realistic model for $\hat{\tau}_S$, also give film heights which are too small. It is concluded that stability theory, as formulated in [19] and [20] and by Craik, does not predict the observed critical conditions for a 2.54 cm channel.

A comparison of figures 16 and 7 shows that the "slow waves" occur at very different conditions, $U_G = 450$ cm/s and $\bar{h} = 0.02$ to 0.06 cm, than used in the experiments discussed in this paper, $U_G = 4500$ cm/s and $\bar{h} = 0.005$ to 0.0015 cm. This would suggest that the "slow waves" might not be the same as the capillary ripples.

5. DISCUSSION

(a) Measurements of wavelengths

The range of wavelengths shown in tables 1–3 reveals that the waves are capillary waves and are not affected by gravity. The values of $\alpha\bar{h}$ are given as 0.13–0.26 in tables 1 and 2 and as

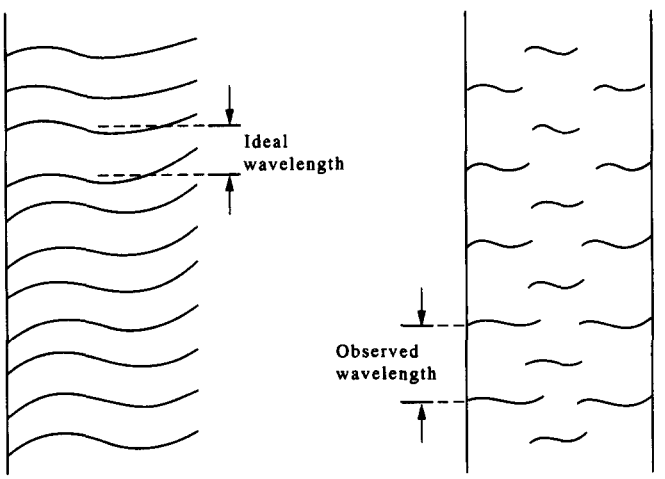

(a) Ideal ripples (b) Observed ripples

Figure 16. Postulated growth of infinitesimal two-dimensional ripples into a finite-amplitude three-dimensional wave pattern.

0.16–0.47 in table 3. This supports the development of an integral momentum balance based on a shallow-liquid assumption, [9], that ignores terms of $O(\alpha\bar{h})^2$. The range of $\lambda/\bar{h}$ is 24–28 in tables 1 and 2 and 13–40 in table 3; this supports the use of a pseudo-steady-state approximation to evaluate the wave-induced variations of τ_W and Γ.

The range of $(\alpha\bar{h})\mathrm{Re}_L$ is 1.4–13.4 in tables 1 and 2 and 1.4–22 in table 3. These are large enough to insure that [9] is accurate to $O(\alpha\bar{h})^2$. Furthermore, it is noted that any simplification of [19] and [20] by assuming $(\alpha\bar{h})\mathrm{Re}_L$ is a small number would not be justified. Further discussion of the range of applicability of boundary-layer approximation may be found in the paper by Jurman & McCready (1989).

(b) Stability analysis

The stability analysis is not exact in that it only satisfies integral momentum and mass balances. It is justified provided $(a\bar{h})^2$ is small compared to unity, that $\lambda/\bar{h}$ is large enough that the wave-induced variations of τ_W and Γ are approximated by a pseudo-steady-state approximation, that $\alpha\bar{h}\mathrm{Re}_L$ is order unity and that $\bar{h}/H$ is small enough that $\mathbf{P} \cong 0$. The results are not absolutely correct because the pseudo-steady-state calculation is not exact.

It is, therefore, of interest to compare dispersion relation [10] with the one derived by Craik (1966). Craik used a series method valid for $(\alpha\bar{h})^3 \ll 1$, $\alpha\bar{h}\mathrm{Re}_L < O(1)$ and $\alpha\bar{h}\mathrm{Re}_L|C| < O(1)$. His [6.5] is reproduced below:

$$\frac{6}{5}\left(\frac{C}{\bar{u}_S}-1\right)^2+\frac{7}{8}\left(\frac{C}{\bar{u}_S}-1\right)+3i\left[\alpha\bar{h}\frac{\bar{h}\bar{u}_S}{\nu_L}\right]^{-1}\left(\frac{C}{\bar{u}_S}-1\right)\left[1+\frac{27}{15}(\alpha\bar{h})^2\right]$$

$$=\frac{\alpha^2\sigma\bar{h}}{\rho_L\bar{u}_S^2}+\frac{\bar{h}\hat{P}_S}{\bar{u}_S^2\rho_L}+\frac{g\bar{h}}{\bar{u}_S^2}\sin\beta+\frac{3}{2}i\frac{\hat{\tau}_S}{\rho_L\alpha\bar{u}_S^2}. \quad [30]$$

Here $\bar{u}_S$ is the liquid velocity at the interface and all terms are dimensional.

If [17] and [18] are substituted into [10], the following result is obtained from the momentum integral analyses presented in this paper, if $\bar{\tau}_S$ is set equal to $\mu\bar{u}_S/\bar{h}$:

$$\left(\frac{C}{\bar{u}_S}-1\right)^2+\frac{3}{4}\left(\frac{C}{\bar{u}_S}-1\right)+3i\left[\alpha\bar{h}\frac{\bar{h}\bar{u}_S}{\nu_L}\right]^{-1}\left(\frac{C}{\bar{u}_S}-1\right)$$

$$=\frac{\alpha^2\sigma\bar{h}}{\rho_L\bar{u}_S^2}+\frac{\bar{h}\hat{P}_S}{\bar{u}_S^2\rho_L}+\frac{g\bar{h}}{\bar{u}_S^2}\sin\beta+\frac{\bar{h}}{\bar{u}_S^2}\frac{\hat{P}_S}{\rho_L}+\frac{3}{2}i\frac{\hat{\tau}_S}{\rho_L\alpha\bar{u}_S^2}. \quad [31]$$

The conditions for the derivation of this equation are $(\alpha\bar{h}) \ll 1$, $\alpha\bar{h}\mathrm{Re}_L \geqslant O(1)$. Both [30] and [31] are obtained assuming $\bar{\tau}_S/\bar{\tau}_W \cong 1$ or $\mathbf{P} \cong 0$.

It is noted that if the term containing $(\alpha\bar{h})^2$ is ignored, [30] and [31] are the same except for small differences in the coefficients multiplying the inertia terms. This is surprising since different restrictions on $\alpha\bar{h}\mathrm{Re}_L$ are made. The tentative conclusion is that [6.5] of Craik's (1966) paper can be used for large $\alpha\bar{h}\mathrm{Re}_L$, but that is then only accurate to $O(\alpha\bar{h})$.

(c) Interpretation of capillary ripples

The stability analysis presents a physical interpretation of the capillary ripples observed at high gas velocities that is essentially the same as Craik's (1966) interpretation of the "slow waves" he observed at low gas velocities. The waves evolve from two-dimensional waves that originate from the growth of small disturbances on the liquid film. The growth results from an imbalance between the stabilizing effect of surface tension and the destabilizing effects of inertia, interfacial shear stresses in phase with the wave slope ($\hat{\tau}_{SI}$) and induced interfacial pressures in phase with the wave height ($\hat{P}_{SR}$). The final stationary waves that evolve will receive energy from the air flow through shear stress variations in phase with the wave height ($\hat{\tau}_{SR}$) and pressure variations in phase with the wave slope ($\hat{P}_{SI}$). These waves differ from those observed on thicker layers where wave-induced shear stress variations do not play an important role.

It is argued that the observed distance between wave peaks should be close to the calculated wavelength of maximum growth. The comparison of the calculated $2\lambda_{max}$ with observed

wavelengths in tables 1–3 indicates that the theory correctly predicts the observed trends in the measurements.

The fact that there is not an exact agreement between the predicted and measured wavelengths should not be surprising because the observed waves, although broad-crested, are not two-dimensional. However, the result that the measurement is equal to twice the prediction is of interest. A possible explanation is that the ripples evolve from a two-dimensional wave with a wavelength equal to the fastest growing wave predicted by linear theory. As these waves grow in amplitude they become unstable to a spanwise disturbance, as shown in figure 16. According to this picture the two-dimensional waves are altered in such a way that the crests break into a group of isolated long-crested three-dimensional waves. Such an instability has been explored by McLean *et al.* (1981) for gravity waves on deep fluids. They found that when the steepness ratio of a two-dimensional wave reaches a value of 0.13 a transition to a three-dimensional wave pattern, with a wavelength in the x-direction twice that of the original wave, is possible.

Acknowledgements—This work was supported by the National Science Foundation under Grant NSF CPE 82-198605 and by the Department of Energy under Grant DEF G02-86ER 13556.

REFERENCES

ABRAMS, J. 1984 Turbulent flow over small amplitude solid waves. Ph.D. Dissertation, Univ. of Illinois, Urbana, IL.

ABRAMS, J. & HANRATTY, T. J. 1984 Relaxation effects observed for turbulent flow over a wavy surface. *J. Fluid Mech.* **151,** 443–455.

ALEKSEENKO, S. V., NAKORYAKOV, V. E. & POKUSAVEV, B. G. 1985 Wave formation on vertical falling liquid films. *Int. J. Multiphase Flow* **11,** 607–627.

ANDRITSOS, N. & HANRATTY, T. J. 1987 Influence of interfacial waves is stratified gas–liquid flows. *AIChE Jl* **33,** 444–454.

ASALI, J. C. 1984 Entrainment in vertical gas–liquid annular flow. Ph.D. Dissertation, Univ. of Illinois, Urbana, IL.

ASALI, J. C., ANDREUSSI, P. & HANRATTY, T. J. 1985 Interfacial drag and film height for vertical annular flow. *AIChE Jl* **31,** 895–902.

BENJAMIN, T. B. 1959 Shearing flow over a wavy boundary. *J. Fluid Mech.* **6,** 161–205.

BONTOZOGLOU, V. & HANRATTY, T. J. 1989 Wave height estimation in stratified gas–liquid flows. *AIChE Jl* **35,** 1346–1350.

COHEN, L. S. & HANRATTY, T. J. 1965 Generation of waves in the concurrent flow of air and a liquid. *AIChE Jl* **11,** 138–144.

CRAIK, A. D. D. 1966 Wind-generated waves in thin liquid films. *J. Fluid Mech.* **26,** 369–392.

HANRATTY, T. J. 1983 Interfacial instabilities caused by air flow over a thin liquid layer. In *Waves on Fluid Interfaces* (Edited by MEYER, R. E.), pp. 221–259. Academic Press, New York.

HANRATTY, T. J. 1991 Separated flow modeling and interfacial transport phenomena. *Appl. Scient. Res.* **48,** 353–390.

HEWITT, G. F. & HALL-TAYLOR, N. S. 1970 *Annular Two-phase Flow*. Academic Press, London.

JURMAN, L. A. & MCCREADY, M. J. 1989 Study of waves on thin liquid films sheared by turbulent gas flow. *Phys. Fluids* **A1,** 522–536.

JURMAN, L. A., BRUNO, K. & MCCREADY, M. J. 1989 Periodic and solitary waves on thin horizontal, gas-sheared liquid films. *Int. J. Multiphase Flow* **15,** 371–384.

LIGHTHILL, M. J. & WHITMAN, G. B. 1955 On kinematic waves. *Proc. R. Soc. Lond.* **A229,** 281–345.

LOYD, R. J., MOFFAT, R. J. & KAYS, W. M. 1970 The turbulent boundary on a porous plate: an experimental study of the fluid dynamics with strong favorable pressure gradients and blowing. Report No. HMT-13, Stanford Univ., CA.

MCLEAN, J. W., MA, Y. C., MARTIN, D. V., SAFFMAN, P. G. & MCLEAN, H. C. 1981 Three-dimensional instability of finite amplitude water waves. *Phys. Rev. Lett.* **46,** 817–820.

SHEARER, C. J. & NEDDERMAN, R. M. 1965 Pressure gradient and liquid film thickness in cocurrent upwards flow of gas/liquid mixtures: application to film-cooler design. *Chem. Engng Sci.* **20,** 671–683.

TAYLOR, G. I. 1963 Generation of ripples by wind blowing over a viscous fluid. In *The Scientific Papers of Sir Geoffrey Ingram Taylor* (Edited by BATCHELOR, G. K.). Cambridge Univ. Press, U.K.

THORSNESS, C. B., MORRISROE, P. E. & HANRATTY, T. J. 1978 A comparison of linear theory with measurements of the variation of shear stress along a solid wave. *Chem. Engng Sci.* **33,** 579–592.

WÜRZ, D. E. 1977 Flüssigkeits—Filmströmung unter einwirkung einer uberschall-luftströmung. Thesis, Institut fur thermische Strömung maschinen, Univ. Karlsruhe.